Available online at www.sciencedirect.com

ScienceDirect

Procedia Engineering 199 (2017) 3047–3052

Procedia Engineering

www.elsevier.com/locate/procedia

X International Conference on Structural Dynamics, EURODYN 2017

Estimation of the dynamic response of a slender suspension bridge using measured acceleration data

Øyvind Wiig Petersen[a,*], Ole Øiseth[a], Eliz-Mari Lourens[b]

[a]*NTNU, Norwegian University of Science and Technology, Department of Structural Engineering, 7491 Trondheim, Norway*
[b]*Delft University of Technology, Faculty of Civil Engineering and Geosciences, 2628 CN Delft, The Netherlands*

Abstract

Suspension bridges with very long spans and slender designs are susceptible to large-amplitude dynamic excitation. Monitoring systems installed on bridges can provide measurement data (e.g. accelerations) and therewith valuable information on the true dynamic behaviour. This pilot study examines the possible use of recently developed methods for real-time response estimation at unmeasured locations. The methodology for response estimation is tested in a case study on the Hardanger Bridge, a 1310 m long suspension bridge in Norway, which has a network of twenty accelerometers. Two techniques, a joint input-state estimation algorithm (JIS) and a dual Kalman filter (DKF), are used to estimate the full-field dynamic response using data measured at the bridge and a reduced order structural model. The results show that the DKF is able to estimate accelerations fairly accurately. The JIS estimate, however, suffer from ill-conditioning and consequently show severe errors. Possible reasons for this ill-conditioning are briefly discussed.

Peer-review under responsibility of the organizing committee of EURODYN 2017.

Keywords: suspension bridge, wind engineering, structural monitoring, response estimation

1. Introduction

Full-scale ambient vibration testing of bridges has already been going on for decades [1,2] and continuous monitoring of structures has become a well-known activity in experimental structural dynamics. Reviews of structural monitoring of bridges can be found in Cunha et al.[3] and Caetano et al.[4]. The applications range from checking vibration serviceability limits [5] and fatigue prediction [6] to studying the ambient load conditions in relation to dynamic response [7–9]. Frameworks for structural health monitoring (SHM) systems is rapidly developing [10], where the idea is to use the measurement data for determining the current state of the system's health. Recent examples of SHM in large structures using vibration data can be found for cable-stayed and suspension bridges in [11–13].

The design of monitoring systems is often restricted by limitations in the number of available sensors, either due to cost or practical operational factors (installation, maintenance or implementation). The reconstruction of structural responses at unmeasured locations based on a limited set of measured data is therefore an appealing goal. Real-time

* Corresponding author. Fax: (+47) 73 59 47 01.
E-mail address: ovyind.w.petersen@ntnu.no

1877-7058
Peer-review under responsibility of the organizing committee of EURODYN 2017.
10.1016/j.proeng.2017.09.547

prediction of response has been done for example with the help of influence lines [14] or novel methods for system inversion [6,15–17].

Novel and complex structures which advance the existing frontiers (in terms of design concepts, span lengths or material use) often make interesting case studies for monitoring, not only for reasons of structural safety, but also to better understand the behaviour of these structures. We present a pilot case study of the Hardanger Bridge (Norway), a slender suspension bridge with a main span of 1310 m. A monitoring system is installed at the bridge, including a network of accelerometers. In this contribution the aim is to estimate the acceleration response at unmeasured locations, which could be implemented as part of a SHM scheme. For this purpose, state of the art techniques for system inversion are employed: a dual Kalman Filter (DKF) [18] and a joint input-state estimation algorithm (JIS) [19,20]. The methods make use of measured acceleration data together with a reduced order structural model.

2. System model equations and identification algorithms

The equations of motion for a suspension bridge modelled with $\mathrm{n_{DOF}}$ degrees of freedom (DOFs) can be written as:

$$\mathbf{M}_0\ddot{\mathbf{u}}(t) + \mathbf{C}_0\dot{\mathbf{u}}(t) + \mathbf{K}_0\mathbf{u}(t) = \mathbf{f}(t) \tag{1}$$

where $\mathbf{u}(t) \in \mathbb{R}^{\mathrm{n_{DOF}}}$ is the response vector. $\mathbf{M}_0$, $\mathbf{C}_0$ and $\mathbf{K}_0 \in \mathbb{R}^{\mathrm{n_{DOF}}\times\mathrm{n_{DOF}}}$ are the mass, damping and stiffness matrices related to the structure only. Static and vortex-induced loads are not considered in this contribution. The load vector $\mathbf{f}(t) \in \mathbb{R}^{\mathrm{n_{DOF}}}$ can then be expanded as follows:

$$\mathbf{f}(t) = \mathbf{C}_{\mathrm{ae}}\dot{\mathbf{u}}(t) + \mathbf{K}_{\mathrm{ae}}\mathbf{u}(t) + \mathbf{f}_{\mathrm{B}}(t) \tag{2}$$

Here, the two first terms on the right hand side represent the motion induced forces, while $\mathbf{f}_{\mathrm{B}}(t)$ is the buffeting wind load. The dynamic response commonly has contributions from a limited number of vibration modes. The following eigenvalue problem is solved to obtain the so-called still-air modes, where only the structural mass and stiffness is considered:

$$(\mathbf{K}_0 - \omega_j^2\mathbf{M}_0)\boldsymbol{\phi}_j = \mathbf{0} \quad (j = 1 \ldots \mathrm{n_m}) \tag{3}$$

The modal transformation $\mathbf{u}(t) = \boldsymbol{\Phi}\mathbf{z}(t)$ is used to establish a reduced order model containing $\mathrm{n_m}$ modes. $\mathbf{z}(t) \in \mathbb{R}^{\mathrm{n_m}}$ is the vector of still-air modal coordinates and $\boldsymbol{\Phi} \in \mathbb{R}^{\mathrm{n_{DOF}}\times\mathrm{n_m}}$ contains the corresponding mass-normalized mode shapes. The modal form of Eq. 1 now reads:

$$\ddot{\mathbf{z}}(t) + \boldsymbol{\Gamma}\dot{\mathbf{z}}(t) + \boldsymbol{\Omega}^2\mathbf{z}(t) = \boldsymbol{\Phi}^{\mathrm{T}}\mathbf{f}(t) = \mathbf{p}(t) \tag{4}$$

where $\boldsymbol{\Omega} = \mathrm{diag}(\omega_1, \omega_2, \ldots, \omega_{\mathrm{n_m}})$ and $\boldsymbol{\Gamma} = \mathrm{diag}(2\omega_1\xi_1, 2\omega_2\xi_2, \ldots, 2\omega_{\mathrm{n_m}}\xi_{\mathrm{n_m}})$; ω_j and ξ_j being the undamped natural frequency and damping ratio for mode j, respectively. Note that Eq. 4 assumes the structural damping ($\mathbf{C}_0$) is proportional. $\mathbf{p}(t) \in \mathbb{R}^{\mathrm{n_m}}$ are now regarded as the unknown modal forces in the system. A discrete time state-space representation of Eq. 4 is introduced with a sample rate of $F_s = (\Delta t)^{-1}$ and a zero order hold on the force:

$$\mathbf{x}_{k+1} = \mathbf{A}\mathbf{x}_k + \mathbf{B}\mathbf{p}_k, \quad \mathbf{x}_k = \begin{pmatrix}\mathbf{z}(t_k)\\ \dot{\mathbf{z}}(t_k)\end{pmatrix}, \quad \mathbf{p}_k = \mathbf{p}(t_k) \tag{5}$$

Here, $\mathbf{x}_k$ is the modal state vector and $\mathbf{p}_k$ is the modal force vector at time $t_k = k\Delta t$ ($k = 1 \ldots N$). It can be shown that the state transition matrix $\mathbf{A} \in \mathbb{R}^{2\mathrm{n_m}\times 2\mathrm{n_m}}$ and input matrix $\mathbf{B} \in \mathbb{R}^{2\mathrm{n_m}\times\mathrm{n_m}}$ are given as:

$$\mathbf{A} = \exp\Big(\begin{bmatrix}\mathbf{0} & \mathbf{I}\\ -\boldsymbol{\Omega}^2 & -\boldsymbol{\Gamma}\end{bmatrix}\Delta t\Big), \quad \mathbf{B} = (\mathbf{A} - \mathbf{I})\begin{bmatrix}\mathbf{0} & \mathbf{I}\\ -\boldsymbol{\Omega}^2 & -\boldsymbol{\Gamma}\end{bmatrix}^{-1}\begin{bmatrix}\mathbf{0}\\ \mathbf{I}\end{bmatrix} \tag{6}$$

We now consider $\mathrm{n_{d,a}}$ acceleration outputs measured at selected DOFs of the structure. The acceleration output vector $\mathbf{y} \in \mathbb{R}^{\mathrm{n_{d,a}}}$ reads:

$$\mathbf{y}_k = \mathbf{S}_{\mathrm{a}}\ddot{\mathbf{u}}(t_k) = \mathbf{G}\mathbf{x}_k + \mathbf{J}\mathbf{p}_k, \quad \mathbf{G} = -\mathbf{S}_{\mathrm{a}}\boldsymbol{\Phi}\begin{bmatrix}\boldsymbol{\Omega}^2 & \boldsymbol{\Gamma}\end{bmatrix}, \quad \mathbf{J} = \begin{bmatrix}\mathbf{S}_{\mathrm{a}}\boldsymbol{\Phi}\end{bmatrix} \tag{7}$$

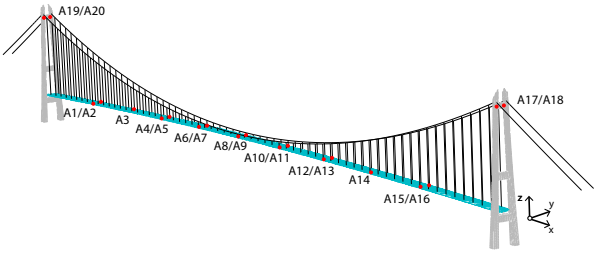

Fig. 1. Location of accelerometers installed at the bridge.

where $\mathbf{S}_\mathrm{a} \in \mathbb{R}^{\mathrm{n_{d,a}} \times \mathrm{n_{DOF}}}$ is a binary selection matrix. $\mathbf{G} \in \mathbb{R}^{\mathrm{n_{d,a}} \times \mathrm{n_m}}$ and $\mathbf{J} \in \mathbb{R}^{\mathrm{n_{d,a}} \times \mathrm{n_m}}$ symbolizes the output influence matrix and direct transmission matrix. Zero mean white noise vectors are added to Eq. 5 and 7, which renders a stochastic state-space representation:

$$\mathbf{x}_{k+1} = \mathbf{A}\mathbf{x}_k + \mathbf{B}\mathbf{p}_k + \mathbf{w}_k \tag{8}$$

$$\mathbf{y}_k = \mathbf{G}\mathbf{x}_k + \mathbf{J}\mathbf{p}_k + \mathbf{v}_k \tag{9}$$

The process noise $\mathbf{w}_k$ and measurement noise $\mathbf{v}_k$ are assumed to have the following covariance relations:

$$\mathbb{E}[\mathbf{w}_k \mathbf{w}_l^\mathrm{T}] = \mathbf{Q}\,\delta_{kl} \quad , \quad \mathbb{E}[\mathbf{v}_k \mathbf{v}_l^\mathrm{T}] = \mathbf{R}\,\delta_{kl} \quad , \quad \mathbb{E}[\mathbf{w}_k \mathbf{v}_l^\mathrm{T}] = \mathbf{S}\,\delta_{kl} \tag{10}$$

Additionally, the random walk force evolution in Eq. 11 is assumed for the DKF, where $\mathbb{E}[\boldsymbol{\eta}_k \boldsymbol{\eta}_l^\mathrm{T}] = \mathbf{Q}_p \delta_{kl}$ is the covariance parameter controlling the allowable step size.

$$\mathbf{p}_{k+1} = \mathbf{p}_k + \boldsymbol{\eta}_k \tag{11}$$

Two algorithms will be used for the response estimation; a joint-input state estimation algorithm [19,20] and the Dual Kalman Filter [18]. Both methods are based on principles of minimum-variance unbiased estimation. For the sake of brevity the filter equations are omitted in this paper. It is recommended to look into the referred original works. Through the use of the measurement data and state space model, the algorithms recursively calculate state estimates ($\hat{\mathbf{x}}_k$) and input estimates ($\hat{\mathbf{p}}_k$). Using the obtained state and input estimates, the acceleration response in any DOF can now be predicted:

$$\hat{\mathbf{y}}_k = \mathbf{S}'_\mathrm{a} \hat{\hat{\mathbf{u}}}_k = \mathbf{G}' \hat{\mathbf{x}}_k + \mathbf{J}' \hat{\mathbf{p}}_k \tag{12}$$

where $\mathbf{S}'_\mathrm{a}$ selects the DOFs of interest, and $\mathbf{G}'$ and $\mathbf{J}'$ is calculated using Eq. 7.

3. System model and monitoring system

The dynamic behaviour of the bridge and ambient wind is monitored by an extensive system consisting of 20 triaxial accelerometers and 9 sonic anemometers. The accelerometers are located in the girder and at the top of the pylons; see Fig. 1 for a layout. Details of the system is featured in Fenerci et al.[7].

The structural model is created in the finite element software Abaqus. Quadrilateral shell elements (S4R) is used for the steel box girder, stiffeners, internal diaphragms as well as the concrete pylons. 2-node Timoschenko beam elements (B31) is used to model the cables, taking into account the important geometric stiffness from the cable tension. Selected modes from the model is shown Fig. 2.

The modes in the reduced order model should represent the dynamic behaviour observed in the measurement data. Fig. 3 shows the acceleration spectral density at the girder mid span. A great number of modes contributes to the total response, however in this work it is decided to focus on the low-frequent dynamics. Thus only modes below 1 Hz with a significant deflection in the girder or pylons are considered as candidates for the model. The $\mathrm{n_m} = 25$ modes listed in Tab. 1 are included in the reduced order model. 7 of the modes are horizontal bending modes, 14 are vertical bending modes, while the remaining modes are either torsion modes (3) and pylon modes (1). The state space model and sensor network used complies with the necessary conditions for instantaneous system inversion listed in [21], except that instabilities in the state and input estimates can occur, since acceleration measurements cannot account for (quasi-)static behaviour.

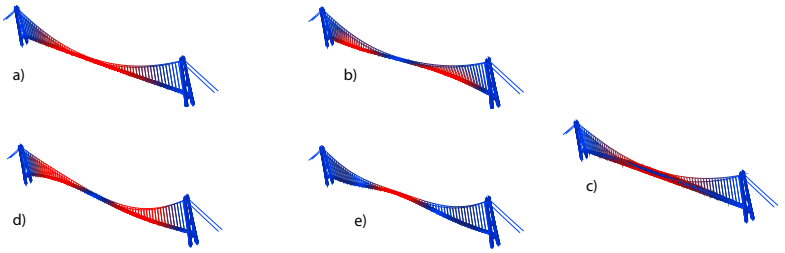

Fig. 2. Still-air modes of the finite element model: a) H1; b) H2; c) T1; d) V1; e) V2.

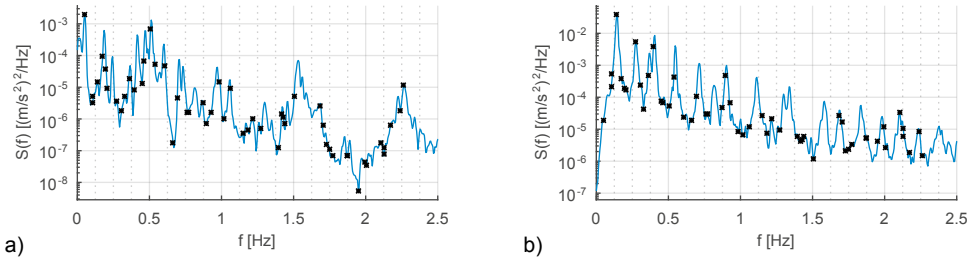

Fig. 3. Auto spectral density of the response at mid span: a) horizontal acceleration; b) vertical acceleration. A Welch average has been used to estimate the spectra. The black dots represent the natural frequencies of the FE model.

Table 1. List of modes included in the reduced order model and their natural frequencies. H=horizontal bending, V=vertical bending, T=torsion, P=pylon.

Mode type	f_j [Hz]	Mode type (cont.)	f_j [Hz]	Mode type (cont.)	f_j [Hz]
H1	0.051	V6	0.331	H6	0.694
H2	0.105	T1	0.371	V11	0.709
V1	0.111	V7	0.400	V12	0.786
V2	0.141	H5	0.462	T3	0.826
H3	0.185	V8	0.465	V13	0.892
V3	0.200	P1	0.507	H7	0.940
V4	0.211	V9	0.544	V14	0.962
V5	0.276	T2	0.551	-	-
H4	0.318	V10	0.621	-	-

4. Response estimation and discussion

A recording from January 26th 2016 with a duration of 30 minutes is selected for this study, during which the mean wind velocity was 12 m/s. A Chebyshev low-pass filter with a cut-off at 1.1 Hz is applied to the acceleration data, which is resampled at 20 Hz. Signals which are numerically redundant (e.g. y-direction for sensor pairs) or insignificant (e.g. z-direction for the pylon sensors) are removed from the sensor network. The acceleration signals A3-y and A14-z (see Fig. 1) are used as reference signals and therefore left out of the sensor network. The remaining sensor network consists of $n_{d,a} = 36$ acceleration outputs.

The matrix $\mathbf{R}$ is taken proportional to the output data: $R_{(i,i)} = \alpha_i^2 \mathrm{Cov}[y_i(t)]$, where the scale factor α_i=0.2 is used for the x-signals, and $\alpha_i = 0.1$ is used for the y- and z-signals. We assume $\mathbf{S}$ of Eq. 10 is zero, while the matrices $\mathbf{Q}$ and $\mathbf{Q}_p$ are tuned manually, based on the expected level of modal excitation:

$$Q_{(j,j)} = Q_{(j+n_m, j+n_m)} = \begin{cases} 0.1 & j = 1 \dots 8 \\ 0.001 & j = 9 \dots 25 \end{cases} \qquad Q_{p,(j,j)} = \begin{cases} 0.1 & j = 1 \dots 8 \\ 0.001 & j = 9 \dots 25 \end{cases} \tag{13}$$

Note that the obtained input and state estimates are more sensitive to $\mathbf{Q}_p$, which controls the input norm, than to $\mathbf{Q}$, which controls the level of process noise, e.g. model errors. Fig. 4 and 5 and shows the estimated accelerations at

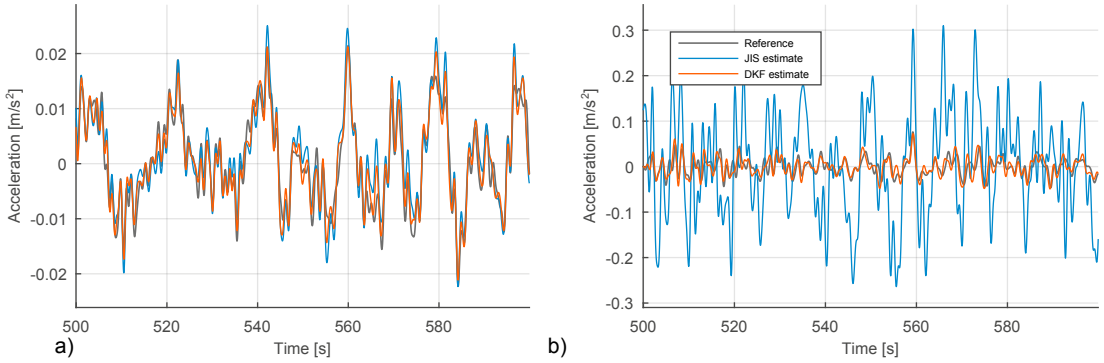

Fig. 4. Time detail ($t \in 500 - 600$ s) of acceleration response estimates and reference signal: a) A3-y (horizontal) ; b) A14-z (vertical).

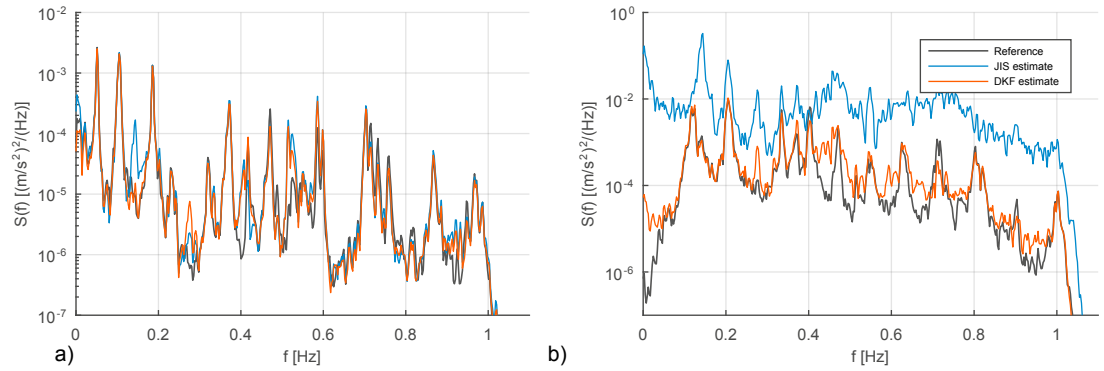

Fig. 5. Auto spectral density (Welch average) of the estimated acceleration: a) A3-y (horizontal) ; b) A14-z (vertical).

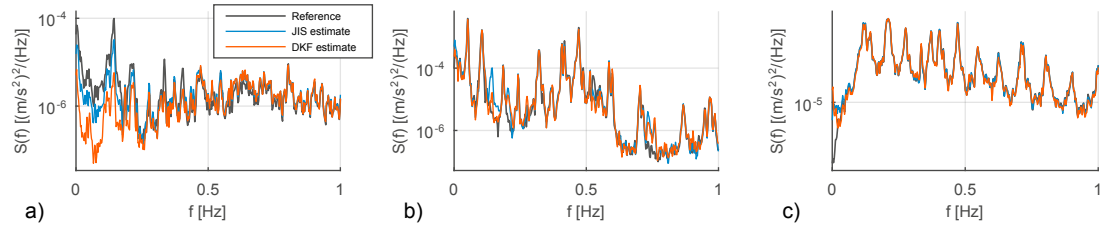

Fig. 6. Auto spectral density (Welch average) of the innovation terms: a) A5-x (longitudinal) ; a) A5-y (horizontal) ; c) A5-z (vertical).

the sensor locations A3 and A14 as predicted using Eq. 12. The DKF estimate generally agrees with the reference, although slightly larger errors are observed for the z-direction. Even though the JIS estimate correctly estimates the acceleration in the y-direction, severe errors occur for the A14-z estimate. Ill-conditioning of the matrices in the system inversion is likely the reason.

Some practical reasons for the ill-conditioning can be elaborated upon. Inverse problems are by nature ill-posed, which means that they are sensitive to errors and noise. The algorithms behind the JIS (cf. [19,20]) and DKF (cf. [18]) are structured differently. The matrix $\mathbf{G}$ in Eq. 7, related to system observability, is involved in more inverse operations in the JIS algorithm than for the DKF. This means that for the JIS estimates, errors tend to magnify when $\mathbf{G}$ is not well-conditioned, which can happen when the outputs are almost linearly dependent on the states. For the considered structure the modes are close to symmetric or antisymmetric, implying that the symmetric sensor layout is inherently less robust to linear dependencies between the different acceleration outputs. The current sensor network layout is not optimal for system inversion applications. We emphasize that outputs which were fully linearly dependent on the states were removed from the sensor network to begin with.

Fig. 6 also shows the how well the algorithms fit the acceleration at the sensor A5, which is included in the sensor network. The largest discrepancy is seen for the x-direction, which could indicate that the model modes do not sufficiently describe the longitudinal dynamic motions, i.e. model errors are present.

5. Concluding remarks

Recently developed methods for real-time system inversion make it possible to predict the full-field dynamic response of a structure from a limited set of measurements and a modal model of the structure. This methodology was tested in a case study of the Hardanger Bridge, which is instrumented with accelerometers. The results show that the DKF is able to accurately reconstruct the acceleration response at unmeasured locations, while the estimates obtained with the JIS experiences severe errors. The failure to accurately reconstruct the response is mainly attributed to increased ill-conditioning during the system inversion.

References

[1] J. Brownjohn, A. Dumanoglu, R. Severn, C. Taylor, Ambient vibration measurements of the humber suspension bridge and comparison with calculated characteristics, Proc. of the Institution of Civil Engineers (London) 83 (1987) 561–600.
[2] A. M. Abdel-Ghaffar, R. H. Scanlan, Ambient vibration studies of Golden Gate Bridge: I. suspended structure, Journal of Engineering Mechanics 111 (1985) 463–482.
[3] A. Cunha, E. Caetano, F. Magalhães, C. Moutinho, Recent perspectives in dynamic testing and monitoring of bridges, Structural Control and Health Monitoring 20 (2013) 853–877.
[4] E. Caetano, A. Cunha, C. Moutinho, F. Magalhães, Dynamic characterization and continuous dynamic monitoring of long span bridges, in: Multi-Span Large Bridges: International Conference on Multi-Span Large Bridges, 1-3 July 2015, Porto, Portugal, 2015.
[5] Á. Cunha, E. Caetano, C. Moutinho, F. Magalhães, Continuous dynamic monitoring of bridges: Different perspectives of application, in: Advanced Materials Research, volume 745, Trans Tech Publ, 2013, pp. 89–99.
[6] K. Maes, A. Iliopoulos, W. Weijtjens, C. Devriendt, G. Lombaert, Dynamic strain estimation for fatigue assessment of an offshore monopile wind turbine using filtering and modal expansion algorithms, Mechanical Systems and Signal Processing 76-77 (2016) 592–611.
[7] A. Fenerci, O. Øiseth, A. Rönnquist, Long-term monitoring of wind field characteristics and dynamic response of a long-span suspension bridge in complex terrain, submitted to Engineering Structures (2016).
[8] K. A. Kvåle, O. Øiseth, Structural monitoring of an end-supported pontoon bridge, Marine Structures 52 (2017) 188–207.
[9] S. Nakamura, GPS measurement of wind-induced suspension bridge girder displacements, Journal of Structural Engineering 126 (2000) 1413–1419.
[10] C. R. Farrar, K. Worden, An introduction to structural health monitoring, Philosophical Transactions of the Royal Society of London A: Mathematical, Physical and Engineering Sciences 365 (2007) 303–315.
[11] J. Ko, Y. Ni, Technology developments in structural health monitoring of large-scale bridges, Engineering structures 27 (2005) 1715–1725.
[12] S. Cho, H. Jo, S. Jang, J. Park, H.-J. Jung, C.-B. Yun, B. F. Spencer Jr, J.-W. Seo, Structural health monitoring of a cable-stayed bridge using wireless smart sensor technology: data analyses, Smart Structures and Systems 6 (2010) 461–480.
[13] M. Kurata, J. Kim, J. Lynch, G. Van der Linden, H. Sedarat, E. Thometz, P. Hipley, L.-H. Sheng, Internet-enabled wireless structural monitoring systems: development and permanent deployment at the New Carquinez Suspension Bridge, Journal of structural engineering 139 (2012) 1688–1702.
[14] H. Sedarat, I. Talebinejad, A. Emami-Naeini, D. Falck, G. van der Linden, F. Nobari, A. Krimotat, J. Lynch, Real-time estimation of the structural response using limited measured data, in: SPIE Smart Structures and Materials+ Nondestructive Evaluation and Health Monitoring, International Society for Optics and Photonics, 2014, pp. 906311–906311.
[15] Y. Niu, C.-P. Fritzen, H. Jung, I. Buethe, Y.-Q. Ni, Y.-W. Wang, Online simultaneous reconstruction of wind load and structural responses: theory and application to Canton tower, Computer-Aided Civil and Infrastructure Engineering 30 (2015) 666–681.
[16] A. Iliopoulos, R. Shirzadeh, W. Weijtjens, P. Guillaume, D. V. Hemelrijck, C. Devriendt, A modal decomposition and expansion approach for prediction of dynamic responses on a monopile offshore wind turbine using a limited number of vibration sensors, Mechanical Systems and Signal Processing 68-69 (2016) 84–104.
[17] T. S. Nord, O. Øiseth, E. Lourens, Ice force identification on the Nordströmsgrund lighthouse, Computers & Structures 169 (2016) 24–39.
[18] S. E. Azam, E. Chatzi, C. Papadimitriou, A dual Kalman filter approach for state estimation via output-only acceleration measurements, Mechanical Systems and Signal Processing 60 (2015) 866–886.
[19] E. Lourens, C. Papadimitriou, S. Gillijns, E. Reynders, G. De Roeck, G. Lombaert, Joint input-response estimation for structural systems based on reduced-order models and vibration data from a limited number of sensors, Mechanical Systems and Signal Processing 29 (2012) 310–327.
[20] K. Maes, A. Smyth, G. De Roeck, G. Lombaert, Joint input-state estimation in structural dynamics, Mechanical Systems and Signal Processing 70–71 (2015) 445–466.
[21] K. Maes, E. Lourens, K. Van Nimmen, E. Reynders, G. De Roeck, G. Lombaert, Design of sensor networks for instantaneous inversion of modally reduced order models in structural dynamics, Mechanical Systems and Signal Processing 52 (2014) 628–644.